Spectroscopical and mechanical characterization of normal and thalassemic red blood cells by Raman Tweezers

Anna Chiara De Luca, [1,2] **Giulia Rusciano,** [1,2*] **Rosanna Ciancia,** [3] **Vincenzo Martinelli,** [3] **Giuseppe Pesce,** [1,4] **Bruno Rotoli,** [3] **Lara Selvaggi,** [1] **Antonio Sasso,** [1,2]

[1] *Dipartimento di Scienze Fisiche, Università di Napoli "Federico II", Complesso Universitario Monte S. Angelo, Via Cinthia, 80126 Napoli, Italy*

[2] *CNISM - Consorzio Nazionale Interuniversitario per le Scienze Fisiche della Materia - Sede di Napoli*

[3] *Hematology Unit, Biochemistry and Medical Biotechnology Department Università degli Studi di Napoli Federico II, Napoli, Italy*

[4] *CNR - Coherentia - Unità di Napoli*

[*] *Corresponding author: giulia.rusciano@na.infn.it*

Abstract: In this work, the effects of thalassemia, a blood disease quite diffuse in the Mediterranean sea region, have been investigated at single cell level using a Raman Tweezers system. By resonant excitation of hemoglobin Raman bands, we have examined the oxygenation capability of β-thalassemic erythrocytes. A reduction of this fundamental erythrocyte function has been found. The measurements have been performed on a significant number of red blood cells; the relative statistical analysis is presented. Moreover, the response to photo-induced oxidative stress of diseased cells with respect to the normal ones has been analyzed. Finally, the deformability of thalassemic erythrocytes has been quantified by measuring the membrane shear modulus by using a double-trap system: the measurements have revealed an increase in membrane rigidity of more than 40%, giving evidence that the genetic defect associated to thalassemia, which manly relies on hemoglobin structure, also strongly affects the erythrocyte mechanical properties. Our results demonstrate that the developed set-up may have potential for the monitoring of blood diseases and their response to drug therapies.

OCIS codes: (170.4520) Optical confinement and manipulation; (170.5660) Raman Spectroscopy; (170.1470) Blood or tissue constituent monitoring.

References and links

1. A. Ashkin, J. M. Dziedzic, J. E. Bjorkholm and S. Chu, "Observation of a single-beam gradient force optical trap for dielectric particles," Opt. Lett. **11,** 288–290 (1986).
2. A. Ashkin and J. M. Dziedzic, "Optical trapping and manipulation of virus and bacteria," Science **235,** 1517–1520 (1987).

#91619 - $15.00 USD Received 15 Jan 2008; revised 25 Feb 2008; accepted 2 Mar 2008; published 19 May 2008

3. K. Svoboda, C. F. Schmidt, D. Branton and S. M. Block, "Conformation and elasticity of the isolated red blood cell membrane skeleton," Biophys. J. **63,** 784–793 (1992).
4. R. Petry, M. Schmitt and J. Popp, "Raman spectroscopy - a prospective tool in the life sciences," Chem. Phys. Chem. **4,** 15–30 (2003).
5. P. J. Lambert, A. G. Whitman, O. F. Dyson and S. M. Akula, "Raman spectroscopy: the gateway into tomorrow's virology," J. Virol. **3,** 1–8 (2006).
6. C. M. Harris, "Raman revisited," Anal Chem. **74,** 433A–438A (2002).
7. M. Dekker, *Infrared and Raman spectroscopy of biological materials,* (H.U. Gremlich and B. Yan, New York, 2001).
8. J. M. Salter, "The effect of radiation trapping of high intensity scattered radiation on multiphoton ionization rates and resonance fluorescence," J. Phys. B: Atom. Molec. Phys. **12,** L763–L767 (1979).
9. Y. Liu, G. J. Sonek, M. K. Berns, K. Konig and B. J. Brock, "Two-photon fluorescence excitation in continuous-wave infrared optical tweezers," Opt. Lett. **20,** 2246–2248 (1995).
10. M. P. Houlne, C. M. Sjostrom, R. H. Uibel, J. A. Kleimeyer and J. M. Harris, "Confocal Raman Microscopy for Monitoring Chemical Reactions on Single Optically Trapped, Solid-Phase Support Particles," Anal. Chem. **74,** 4311–4319 (2002).
11. J. C. Carls, G. Monaivais and J. R. Brock, "Time-resolved Raman Spectroscopy from reacting optically levitated microdroplets," Appl. Opt. **29,** 2913–2918 (1990).
12. M. Lankers, J. Popp and W. Kiefer, "Raman and Fluorescence Spectra of Single Optically-Trapped Microdroplets in Emulsionsby," Appl. Spectrosc. **48,** 1166–1168 (1994).
13. K. Ajito, "Combined Near-Infrared Raman Microprobe and Laser Trapping System: Application to the Analysis of a Single Organic Microdroplet in Water," Appl. Spectrosc. **52,** 339–342 (1998).
14. K. Ajito and K. Torimitsu, "Near-infrared Raman spectroscopy of single particles," Trends Anal. Chem. **20,** 255–262 (2001).
15. G. J. Thomas, "Raman spectroscopy of protein and nucleic acid assemblies," Annu. Rev. Biophys. Biomol. Struct. **28,** 1–27 (1999).
16. J. W. Chan, D. S. Taylor, T. Zwerdling, S. M. Lane, K. Ihara and T. Huser, "Micro-Raman spectroscopy detects individual neoplastic and normal hematopoietic cells," Biophys. J. **90,** 648–656 (2006).
17. G. Rusciano, A. C. De Luca, G. Pesce and A. Sasso, "Phase-sensitive detection in Raman tweezers," Appl. Phys. Lett. **89,** 261116–261118 (2006).
18. C. M. Creely, G. P. Singh and D. V. Petrov, "Dual wavelength optical tweezers for confocal Raman spectroscopy," Opt. Commun. **245,** 465–470 (2005).
19. D. Cojoc, E. Ferrari, V. Gabin and E. Di Fabrizio, "Multiple optical tweezers for micro Raman spectroscopy," Proc. SPIE **5930,** 59300B1–11 (2005).
20. P. R. T. Jess, V. Garcs-Chvez, D. Smith, M. Mazilu, L. Paterson, A. Riches, C. S. Herrington, W. Sibbett and K. Dholakia, "Dual beam fibre trap for Raman micro-spectroscopy of single cells," Opt. Express **14,** 5779–5791 (2006).
21. G. P. Singh, G. Volpe, C. M. Creely, H. Grötsch, I. M. Geli and D. Petrov, "The lag phase and G1 phase of a single yeast cell monitored by Raman microspectroscopy," J. Raman Spectrosc. **37,** 858–864 (2006).
22. C. Creely, G. Volpe, G. Singh, M. Soler and D. Petrov, "Raman imaging of floating cells," Opt. Express **13,** 6105–6110 (2005).
23. C. Xie, M. A. Dinno and Y.-Q. Li, "Near-infrared Raman spectroscopy of single optically trapped biological cells," Opt. Lett. **27,** 249–251 (2002).
24. C. Xie and Y.-Q. Li, "Confocal micro-Raman spectroscopy of single biological cells using optical trapping and shifted excitation difference techniques," J. Appl. Phys. **93,** 2982–2986 (2003).
25. C. Xie, C. Goodman, M. Dinno and Y.-Q. Li, "Real-time Raman spectroscopy of optically trapped living cells and organelles," Opt. Express **12,** 6208–6214 (2004).
26. C. Xie, D. Chen and Y.-Q. Li, "Raman sorting and identification of single living micro-organisms with optical tweezers," Opt. Lett. **30,** 1800–1802 (2005).
27. T. G. Spiro and X-Y. Li, *Biological Application of Raman Spectroscopy,* (Wiley, New York, 1988).
28. H. Brunner, A. Mayer and H. Sussner, "Resonance Raman Scattering on the heam group of the oxy- and deoxy-haemogloin," J. Mol. Biol. **70,** 153–156 (1972).
29. B. R. Wood, B. Tait and D. McNaughton, "Micro-Raman characterization of the R to T state transition of haemoglobin within a single living erythrocyte," Biochim. Biophys. Acta **1539,** 58–70 (2001).
30. B. R. Wood, P. Caspers, G. J. Pupples, S. Pandiancherri and D. McNaughton, "Resonance Raman Spectroscopy of red blood cell using near-infrared laser excitation," Anal. Bioanal. Chem. **387,** 1691–1703 (2007).
31. K. Ramser, K. Logg, M. Gokör, M. Käll and D. Hanstorp, "Resonance Raman spectroscopy of optically trapped functional erythrocytes," J. Biomed. Opt. **9,** 593–600 (2004).
32. B. R. Wood and D. McNaughton, "Raman excitation wavelength investigation of single red blood cell in vivo," J. Raman Spectrosc. **33,** 517–523 (2002).
33. I. P. Torres Filho, J. Terner, R. N. Pittman, L. G. Somera and K. R. Ward, "Hemoglobin oxygen saturation measurements using resonance Raman intravital microscopy," Am. J. Physiol. Heart Circ. Physiol. **289,** 488–495

#91619 - $15.00 USD Received 15 Jan 2008; revised 25 Feb 2008; accepted 2 Mar 2008; published 19 May 2008

(2004).
34. K. Ramser, J. Enger, M. Gokör, D. Hanstorp, K. Logg and M. Käll, "A microfluidic system enabling Raman measurements of the oxygenation cycle in single optically trapped red blood cells," Lab Chip **5,** 431–436 (2005).
35. R. L. McCreery, "Raman Shift Frequency Standards: Polystyrene," http://www.chemistry.ohio-state.edu/∼rmccreer/freqcorr/images/poly.html.
36. G. Rusciano, A. C. De Luca, G. Pesce and A. Sasso, "Enhancing Raman Tweezers by phase-sensitive detection," Anal. Chem. **79,** 3708–3715 (2007).
37. M. Abe, T. Kitagawa and Y. Kyogoku, "Resonance Raman spectra of octaethylporphyrinato-Ni(II) and mesodeuterated and 15N substituted derivatives. II. A normal coordinate analysis," J. Chem. Phys. **69,** 4526–4531 (1978).
38. S. Hu, K. M. Smith and T. G. Spiro, "Assignment of Protoheme Resonance Raman Spectrum by Heme Labeling in Myoglobin" J. Am. Chem. Soc. **118,** 12638–12646 (1996).
39. I. Kahane, A. Shifter and E. A. Rachmilewitz, "Cross linking of red blood cells membrane proteins induced by oxidative stress in beta-thalassemia," FEBS Lett. **85,** 267–270 (1978).
40. E. A. Rachmilewitz, B. M. Lubin and S. B. Shohet, "Lipid membrane peroxidation in beta-thalassemia," Blood **47,** 495–505 (1976).
41. E. Shinar, E. A. Rachmilewitz and S. E. Lux, "Differing erythrocyte membrane skeletal protein defects in alpha and beta thalassemia," J. Clin. Invest. **83,** 404–410 (1989).
42. S. K. Boey, D. H. Boal and D. E. Discher, "Simulations of the erythrocyte cytoskeleton at large deformation. I. Microscopic models," Biophys. J. **75,** 1573–1583 (1998).
43. D. E. Discher, D. H. Boal and S. K. Boey, "Simulations of the erythrocyte cytoskeleton at large deformation. II. Micropipette aspiration," Biophys. J. **75,** 1584–1597 (1998).
44. J. Li, M. Dao, C. T. Lim and S. Suresh, "Spectrin-level modeling of the cytoskeleton and optical tweezers stretching of the erythrocyte," Biophys. J. **88,** 3707–3719 (2005).
45. G. Lenormand, S. Hénon, A. Richert and F. Gallet, "Direct measurement of the area expansion and shear moduli of the human red blood cell membrane skeleton," Biophys. J. **81,** 43–56 (2001).
46. S. Hénon, G. Lenormand, A. Richert and F. Gallet, "A new determination of the shear modulus of the human erythrocyte membrane using optical tweezers," Biophys. J. **76,** 1145–1151 (1999).
47. E. A. Evans and N. Mohandas, "Membrane-associated sickle hemoglobin: a major determinant of sickle erythrocyte rigidity," Blood **70,** 1443–1449 (1987).
48. E. A. Evans, "A new membrane concept applied to the analysis of fluid shear- and micropipette-deformed red blood cells," Biophys. J. **13,** 941–954 (1973).
49. D. J. Weatherall and J. B. Clegg, "Thalassemia revisited," Cell **29,** 7–9 (1982).
50. G. Athanasiou, N. Zoubos and Y. Missirlis, "Erytrhrocyte membrane deformability in patients with thalassemia syndromes," Nouv. Rev. Fr. Hematol. **33,** 15–20 (1991).
51. O. Inya-Agha, N. Klauke, T. Davies, G. Smith and J. M. Cooper, "Spectroscopic Probing of Dynamic Changes during Stimulation and Cell Remodeling in the Single Cardiac Myocyte," Anal. Chem. **79,** 4581–4587 (2007).
52. K. Mohanty, S. Mohanty, S. Monajembashi, K. O. O Greulich, "Orientation of erythrocytes in optical trap revealed by confocal fluorescence microscopy," J. Biomed. Opt. **12,** 0605061–0605063 (2007).

1. Introduction

The composition and conformation of biomolecules within a living cell may change in response to external agents, such as environmental stress or drug administration, or in presence of cellular disorders. Rapid identification of these changes, at single cell level, is a challenging topic for many biomedical applications, and for the understanding of fundamental cellular processes.

Optical Tweezers (OT) [1] have revealed to be a powerful tool to address this issue. Based on the use of a strongly focused laser beam, they allow trapping and manipulation of micro-sized objects in absence of mechanical contact [2]. Optical trapping allows cell immobilization without fixing it to a substrate, avoiding adsorption-induced effects. In addition, it becomes possible to apply forces and torques in order to investigate, for instance, elasticity and viscoelasticity of single cells or microrganelles [3].

An interesting trait of OT is that they can be combined with spectroscopic techniques, including absorption, fluorescence, and Raman spectroscopy, in order to extract structural information about single trapped objects [4-9]. Among these, Raman spectroscopy has been widely used for the analysis of biological samples in aqueous solution, thanks to the weak Raman activity of water. Raman spectroscopy is based on the inelastic scattering of radiation; the spectral

#91619 - $15.00 USD Received 15 Jan 2008; revised 25 Feb 2008; accepted 2 Mar 2008; published 19 May 2008

features are straightly connected to the fundamental vibrational modes of the bonds of the analyzed chemical species [10-14]. Nowadays, its range of application is very wide, ranging from the study of protein or nucleic acid [15] to the comparison between normal and neoplastic cells [16].

The combination of an Optical Tweezers with a Raman System (Raman Tweezers, RT) allows getting spectra coming from a single particle instead from an ensemble average [17]. In this way, heterogeneity can be exalted, and information about composition and distribution of specific chemical species can be obtained [18-26].

Several Raman based techniques have been developed to enhance the intensity and improve the spatial resolution with respect to the basic method. In particular, Resonance Raman Spectroscopy (RRS) occurs when the excitation wavelength matches to an electronic transition of the molecule so that vibrational modes associated with the excited electronic state are greatly enhanced. This kind of analysis is particularly useful for investigation of biologically relevant metalloporphyrin complexes, which, due to the presence of large aromatic rings, present absorption bands in the visible region [27]. RRS has been, in fact, widely used to investigate human erythrocytes, also at single cell level.

Erythrocytes, also referred as red blood cells (RBCs), perform the most important blood duty and play an essential role in human respiratory function. They consist mainly of hemoglobin (Hb), a globular protein with an embedded porphyrin (heme group), which constitutes the Hb prosthetic component. Each group contains an iron atom, which temporarily links to oxygen molecules in the lungs and release them throughout the body. The high symmetry and the chromophoric structure of the heme result in strong enhancement of the Raman Scattering using laser wavelengths close to the heme electronic absorption bands [28-31]. The occurrence of resonance Raman scattering from the Hb prostheic group allows the investigation of Hb within erythrocytes without interference by other RBC component scattering [32-34]. This is a quite interesting issue for the characterization of Hb-related blood diseases, such as thalassemias. Thalassemia is a disease of RBC inherited as a semidominant trait, quite diffuse in the populations of the Mediterranean sea. In thalassemia, the genetic defect results in reduced rate of synthesis of one of the globin chains; they are classified according to which chain of the globin molecule is affected: in α-thalassemia, the production of α globin is deficient, while in β-thalassemia the production of β globin is defective. As a consequence, α/β chain ratio is imbalanced, leading to an excess of the normal chain, which may be more injurious to the cell than the defect of the affected chain. Indeed, free globin chains bind to the cell membrane, damaging it and rendering the cell more vulnerable to mechanical injuries. β-thalassemia is the most common of this disease; its incidence can be as high as 1 in 10 in some Mediterranean areas.

In this work we present the results of the characterization of RBC from β-thalassemic patients obtained by using an OT system integrated with a Raman probe. In particular, we compare the Raman spectra of single thalassemic RBCs (t-RBCs) with those obtained from healthy subjects, relating the observed differences to the analyzed disease. We also investigate photo-induced effects caused by the laser radiations used for both trapping and Raman excitation. Finally, we study the mechanical response of normal and thalassemic cells by monitoring the deformation induced by a double-trap system. We think that this work can have significant applications for the characterization of RBC with functional alterations and for a better understanding of the biology of thalassemic RBCs.

#91619 - $15.00 USD Received 15 Jan 2008; revised 25 Feb 2008; accepted 2 Mar 2008; published 19 May 2008

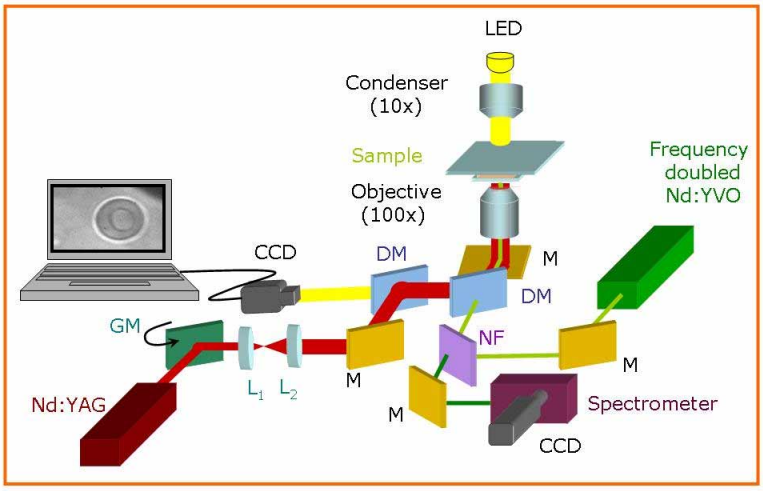

Fig. 1. Experimental set-up of the combined Optical Tweezers and Raman Spectrometer: L, lens; M, mirror; DM, dichroic mirror; GM, galvomirror; NF, notch filter.

2. Materials and methods

2.1. Experimental set-up

Figure 1 illustrates the main components of our experimental set-up which essentially consists of an Optical Tweezers system combined with a Raman spectrometer. The trapping laser was given by a Nd:YAG laser (1064 nm; Laser Quantum, Ventus 1064), emitting a maximum power of 3 W. It was tightly focused into the sample by an Olympus oil-immersion infinity corrected objective lens (100X, 1.4 N.A.). A telescopic system (lenses L_1 and L_2 in Fig. 1), placed at a proper distance from the objective entrance pupil, guaranteed a constant coupling of the trapping beam into the microscope. Resonance Raman spectra of RBCs were excited by a frequency-doubled Nd-YVO laser (532 nm; Spectra Physics Millennia Xs). It was mixed to the trapping beam through a dichroic mirror, reflecting near-IR radiation and being transparent to visible radiation. Back scattered light from the sample, collected and collimated by the same focusing objective, followed back the same path as the incident Raman probe, reaching finally an holographic notch filter. This last reflected the Rayleigh scattered radiation while provided a good transmission of the inelastic scattered Raman light. The so filtered radiation was focused onto the entrance slit (set at an aperture of 50 μm) of the spectrometer (TRIAX 180, Jobin-Yvon), equipped with a 1800 lines/mm holographic grating. Finally, the Raman radiation was detected by using a front-illuminated charge-coupled device (Pixis 1024, Princeton Instruments, 1024 $\times$ 1024 pixels), thermoelectrically cooled at -70 ^{o}C and placed at the spectrometer exit. The detector was interfaced to a personal computer, where spectra were stored and analyzed. To precisely assign a wave number to each individual detector pixel, we used a trapped polystyrene latex beads (SERVA Electrophoresis), whose Raman peaks positions are accurately known [35]. Calibration points distributed over the whole spectral region of interest were fitted by a straight line. The final spectral resolution was 2 cm^{-1}, as estimated from the polystyrene spectrum by measuring the FWHM of the 1001.4 cm^{-1} peak.

#91619 - $15.00 USD Received 15 Jan 2008; revised 25 Feb 2008; accepted 2 Mar 2008; published 19 May 2008

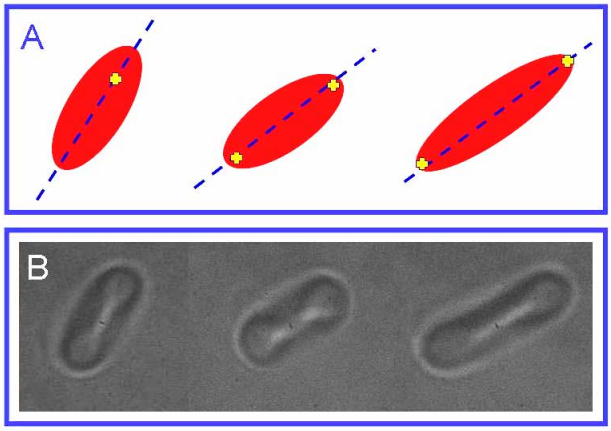

Fig. 2. A: Sketch of the stretching procedure used for the present investigation. B: Same frames of a video recorded during the stretching of a normal RBC.

The light from a LED, focused on the sample by a 10X objective, was used to illuminate the sample; an image of the trapped cell was obtained by using a CCD camera, coupled to the microscope.

The sample chamber was constituted by two 150 μm glass coverslips (Knittel Glasser, thickness no.1), sealed with parafilm stripes which also act as $\sim$ 100 μm spacer. The chamber was placed on a translational stage, providing the sample movement (micrometer translator Newport, HR-13, step size: 2 μm, travel: 13 mm). RBCs were trapped at a distance of about 4 μm from the lower coverslip. At this distance, the optical aberrations are reduced and the Raman collection efficiency is maximized [36].

For the mechanical characterization of RBCs, a double-trap system was created by applying a square voltage signal at a frequency of 1 kHz to a galvomirror (Cambridge Technology Incorporated, mod. 6220), placed on the optical path of the trapping beam. In such a way, the two optical traps shared the beam power and their relative distance was controlled by the voltage signal amplitude.

A sketch of our stretching mechanism is illustrated in Fig. 2(A), while in the part (B) of the same figure some frames of a recorded video are shown. When the voltage applied to the galvomirror is zero, we have a conventional single trap: the RBC reaches a trapped position and floats slightly around it. As the distance between the two traps is increased, the RBC firstly starts orientating along the axis passing through the center of the two traps. After the RBC is fully aligned, it begins to be stretched. RBC elongation was extracted by hand, using an image software (NHI ImageJ). In particular, we recorded 20 images for each erythrocyte elongation. From each image we estimated the major axis of the RBC shape and computed the average length over all the 20 frames.

#91619 - $15.00 USD Received 15 Jan 2008; revised 25 Feb 2008; accepted 2 Mar 2008; published 19 May 2008

2.2. *Sample preparation*

Fresh blood was obtained by fingerprint needle prick. Control samples were drown from six normal adults. All thalassemic consenting (n=6) subjects showed typical pathological features such as reduced MCV (red cell mean corpuscular volume) and elevated HbA2 electrophoresis fraction; serum ferritin was normal in all of them.

Samples were prepared according to the following procedure: blood (5 μl) anticoagulated by K-EDTA, was diluted in 10 ml of isotonic aqueous NaCl solution and 0.5 ml of human albumin (used as membrane protection). Few microliters of this solution were transferred, within few minutes, in a home-made chamber.

3. Results and discussion

3.1. *Resonant Raman spectroscopy.*

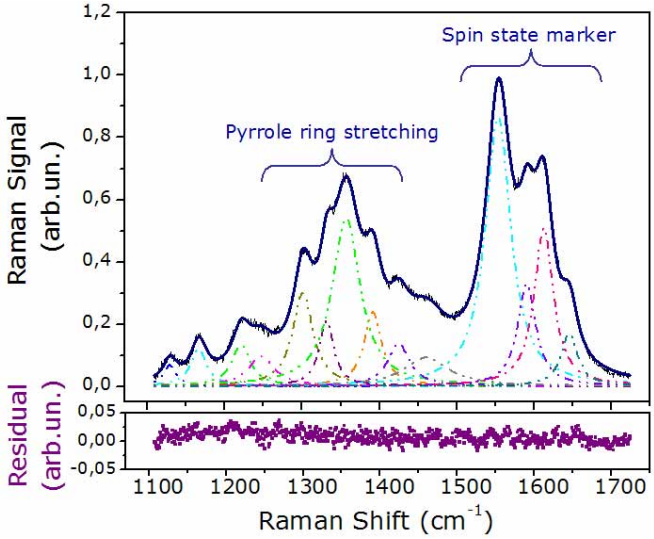

Fig. 3. Upper part: Typical Raman spectrum of an healthy RBC, obtained with an integration time of 10 s. The solid line corresponds to a fitting with 14 Lorentzian profiles, while the dashed lines indicate the deconvoluted curves. Lower part: Residual obtained as the difference between the experimental and the best-fit spectrum.

Figure 3 shows a typical Raman spectrum, between 1100 and 1750 cm $^{-1}$, of a single optically trapped functional erythrocyte from a healthy volunteer. It was obtained with an excitation power of 0.2 mW and an integration time of 10 s. The contribution due to the buffer solution, taken by removing the RBC from the trap, was subtracted. No averaging was performed, in order to minimize the exposition time to the Raman probe and, hence, to reduce photo-induced effects. The obtained Raman bands are due to the resonantly enhanced hemoglobin contribution; in particular, enhancement of the inelastic scattering comes from the coupling of Raman excitation with the porphyrin macrocycle Q band. Although the relative intensity of the different Raman bands are strongly affected by the excitation wavelength [32], numerous spectral features can be clearly identified, according to their spectral positions. Band assignment, reported in Table 1, follows the work by Abe *et al.* [37] and the successive work of Wood *et al.* [32]. For a better estimation of both spectral position and intensity of the observed Raman features, the spectral region between 1100 and 1750 cm $^{-1}$ was fitted with 14 Lorentzian profiles,

#91619 - $15.00 USD Received 15 Jan 2008; revised 25 Feb 2008; accepted 2 Mar 2008; published 19 May 2008

Table 1. Assignment and spectral position (cm^{-1}) of the Hb Raman bands observed in this work. For comparison, we also report the bands observed by Wood et al. [32] for both oxy- and deoxy-Hb with excitation at 514 nm.

Band Assignment [37]	Local coordinate [38]	Hb band position 532 nm	Oxy Hb [32] 514 nm	Deoxy Hb [32] 514 nm
ν_{10}	$\nu(C_\alpha C_m)_{asym}$	1640	1638	Absent
ν_{19}	$\nu(C_\alpha C_m)_{asym}$	1604	1604	1604
ν_{37}	$\nu(C_\alpha C_m)_{asym}$	1588	1585	1580
ν_{11}	$\nu(C_\beta C_\beta)$	1548	1547	1546
-CH_2(scissor)	-CH_2(scissor)	1467	1471	1471
ν_{28}	$\nu(C_\alpha C_m)_{asym}$	1430	1430	1425
ν_{20}	$\nu(pyrquarter-ring)$	1397	1397	1394
ν_4^d	$\nu(pyrhalf-ring)_{sym}$	1356	1356	1356
ν_{41}	$\nu(pyrhalf-ring)_{sym}$	1336	1336	1336
ν_{21}	$\delta(C_mH)$	1301	1301	1301
ν_{13}		1248	1245	Absent
ν_{13} or ν_{42}	$\delta(C_mH)$	1223	1228	1220
ν_{30}	$\nu(pyrhalf-ring)_{asym}$	1170	1171	1172
ν_{22}	$\nu(pyrhalf-ring)_{asym}$	1131	1134	1124

each corresponding to an expected Raman feature [32]. All parameters (intensity, spectral position and width) were allowed to vary in the fitting procedure. The 14 deconvoluted profiles are reported as dashed lines in Fig. 3, while the envelope of this curves is shown with a solid line. As it is possible to see from the residual, calculated as the difference between the experimental and fitted spectra and shown in the lower part of Fig. 3, the Lorentzian profiles approximate quite well the experimental data.

The prominent Raman features occur in the spectral region between 1500 and 1650 cm^{-1}, which corresponds to the *core size* or *spin state marker* band region. As a matter of fact, these strong bands provide information about the Hb oxidation state: when the Fe atom in the porphyrin heterocyclic ring is linked to oxygen, it is in the low spin state (S=1/2), while in the deoxygenated heme, Iron is in the up spin state (S=2). In these two cases, the porphyrin ring exhibits different symmetries, so that the strength and the spectral position of its vibrations are sensitive to the oxygenation condition. This issue has been also pointed out by Wood *et al.* [32] in its investigation on the wavelength dependence of human erythrocyte Raman bands. In particular, the authors found that some Raman peaks were absent in deoxygenated RBC, while others shown a valuable energy shift (see Table 1).

This evidence constitutes the starting point in the interpretation of the erythrocyte Raman spectrum from thalassemic patients. Figure 4 compares the Raman spectrum of a healthy RBC and that corresponding to heterozygous β-thalassemic cells. It is possible to highlight some interesting differences. First of all, Raman bands characteristic of oxygenated Hb (oxyHb) are strongly depressed for the β-thalassemic ones. For instance, the ν_{10} band, clearly visible in the spectrum of normal RBC, can be resolved in the spectrum of thalassemic RBCs only after deconvolution from the stronger ν_{19} band by the fitting procedure.

A quantitative analysis of this effect is shown in Fig. 5, where we compare the intensity of selected Raman features (ν_{37}, ν_{10} and ν_{13} bands), normalized to the ν_{11} band intensity, for healthy and thalassemic cells. Moreover, numerous Raman bands, affected by oxygenation condition, are energy-shifted (see Table 2). Both experimental outcomes clearly mirrors a lower efficiency of t-RBC in carrying out their natural role, namely oxygen transportation from lungs

#91619 - $15.00 USD Received 15 Jan 2008; revised 25 Feb 2008; accepted 2 Mar 2008; published 19 May 2008

to all the organism. To test the reproducibility of these results, we performed a statistical analysis on RBCs, collected from normal individuals and heterozygous thalassemic patients. For each sample we performed the Raman analysis described above, estimating the ratio between the intensity of the ν_{37} and that of the ν_{11} bands ($R = I_{\nu_{37}}/I_{\nu_{11}}$).

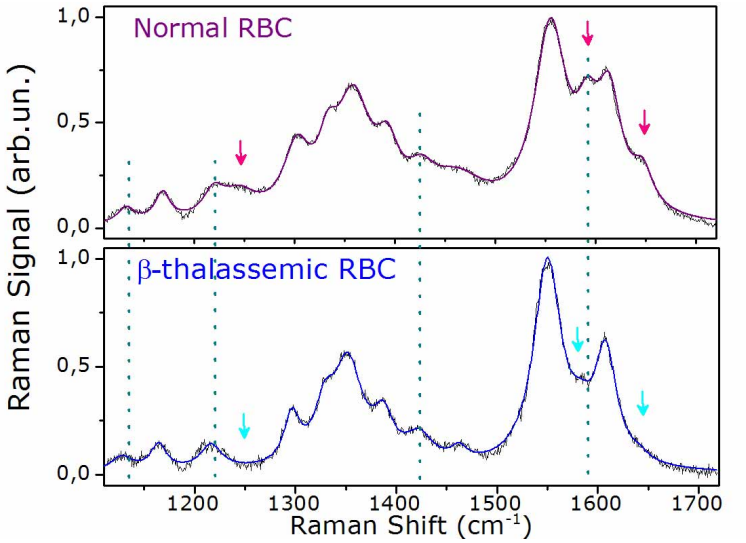

Fig. 4. Comparison between the Raman spectra of normal and β-thalassemic RBC. The arrows indicate the spectral features affected by intensity changes, while the dashed lines highlight the observed energy shift.

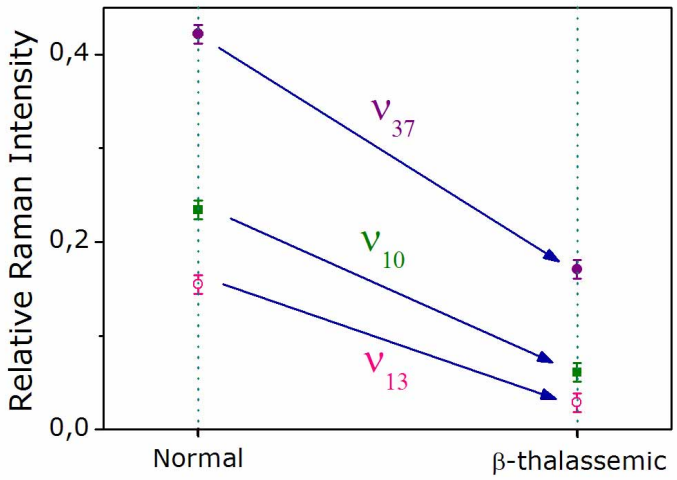

Fig. 5. Trends of the relative intensity for selected Raman peaks (ν_{37}, ν_{10} and ν_{13}) corresponding to the two types of cells (see text for details).

#91619 - $15.00 USD Received 15 Jan 2008; revised 25 Feb 2008; accepted 2 Mar 2008; published 19 May 2008

Table 2. Observed wavenumber (cm^{-1}) relative to 4 Raman peaks for normal and β-thalassemic RBCs.

Band Assignment	Normal	β-thalassemic
ν_{37}	1588	1581
ν_{28}	1430	1426
ν_{13} or ν_{42}	1223	1215
ν_{22}	1131	1125

In Fig. 6(A), we report the statistical distributions of the ratio R corresponding to a normal and a thalassemic donor. Each distribution is relative to 300 spectra. Overlapped to them, we also show the fits with a Gaussian curve. This analysis was repeated for 6 volunteers for each kind of cells (see Fig. 6(B)). From this investigation, two interesting features emerge. First of all, the distributions are well separated; more precisely, they are not overlapping within three standard deviations, as evidenced by the horizontal bars, which show the weighted-mean and the standard deviation for the normal and the thalassemic cells.

In addition, all t-RBCs distributions present a much wider spread around their mean values with respect to that of healthy RBCs. The wider distribution found for diseased RBCs clearly mirror the higher heterogeneity of t-RBCs, which can be also observed in the dimension and shape of these erythrocytes. We think that these experimental outcomes provide an interesting starting point to explore the application of a Raman Tweezers system in the clinical diagnosis of Hb-related blood disorders.

3.2. Photo-induced effects.

During our experiments a particular care was put in order to reduce photo damages induced by the trap and Raman lasers. Indeed, more generally, when biological samples are exposed to laser radiation it is important to be aware of possible photo-induced effects. These last have been investigated for normal RBC exposed to visible and IR radiation [32]. In general, it has been established [32] that exposition to high-power radiation in the green region leads to protein denaturation and Hb transfer into the metHb state, in which the oxygen is irreversibly bound to the heme. In our study we extended this investigation to β-thalassemic erythrocytes. We first analyzed the effects of exposition of both normal and thalassemic RBC to radiation at 1064 nm, which corresponds to the wavelength of our trapping laser. At this purpose, a single erythrocyte was placed in the optical trap for different time intervals, ranging between 20 and 300 s; at the end of each interval, we monitored RBC vitality by recording its Raman spectrum for 3 s. To avoid the superposition of effects induced by the Raman probe, the RBC was changed after each measurement. The power of the IR beam was taken fixed at 15 mW, while the Raman probe power was 0.2 mW.

In Fig. 7 we report the intensity of the ν_{11} peak at 1548 cm^{-1}, normalized at the maximum value (I^{MAX}_{Raman}), for healthy and β-thalassemic RBCs. The latter Raman feature is the stronger one for the two kinds of cells and its relative intensity is not affected by Hb met transition. For each trapping time we repeated ten measurements using distinct cells. The points plotted in Fig. 7 represent the average values while the error bars are the standard deviations. As it can be seen, the normalized Raman intensity changes by 12 % for normal cells and 17 % for the thalassemic ones on a period of 300 s. In addition, we observed that the relative intensities of the different peaks in the Raman spectra were not affected. This indicates that, at power level used in our experiment, the photo-damage by IR laser trapping is quite low.

The photo-induced effects at 532 nm are, instead, much stronger. Figure 8 shows the intensity of the same Raman feature (ν_{11}) as a function of exposure time to the Raman probe, at

#91619 - $15.00 USD Received 15 Jan 2008; revised 25 Feb 2008; accepted 2 Mar 2008; published 19 May 2008

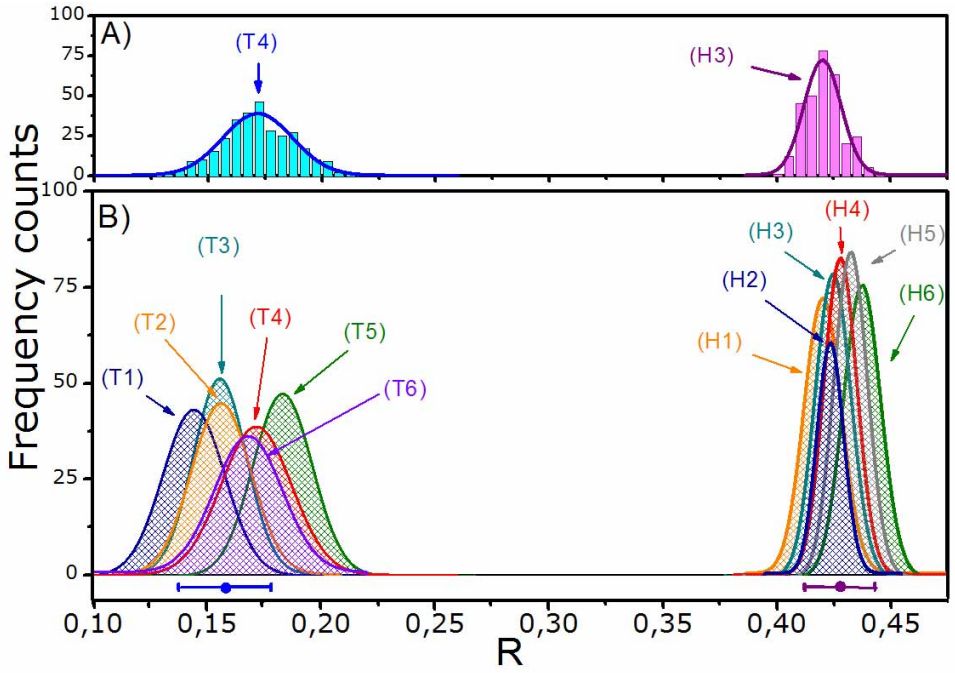

Fig. 6. A: Statistical distributions of the ratio $R = I_{\nu_{37}}/I_{\nu_{11}}$ obtained by analyzing 300 RBCs from a single normal (pink histogram) and thalassemic (blue histogram) donor. The fitting of these distributions with Gaussian profile is also shown. B: Gaussian profiles obtained by fitting the experimental distributions relative to 6 normal (Hi) and 6 thalassemic (Ti) volunteers. The weighted-mean and the standard deviation for the two kinds of cells are evidenced by horizontal bars.

a power of 0.3 mW (the trapping laser power was kept at 15 mW). Again, the measurements were done trapping one fresh cell and exposing it to 532 nm radiation for a time varying from 3 to 150 s. As for Fig. 7, the measurements were normalized to the intensity of the maximum Raman signal, observed at t=3 s.

As it can be observed in Fig. 8, the photo-damage is different for the two kinds of cells. For an exposure time of about 80 s, the reduction of the Raman signal is $\sim$50 % for normal cells and $\sim$80 % for β-thalassemic cells. Therefore, our investigation shows that thalassemic RBCs are more sensitive to photo-oxydation.

This result confirms a more general trend of thalassemic RBCs to be sensitive to oxidant stress [39, 40]. From a medical point of view, this may be attributed to an excessive oxidation of the unstable free globin chains and the subsequent release of oxygen radicals, that might damage the cell membrane [41]. This information has to be taken into account in all optical analysis of t-RBCs.

Another evidence of the photo-damage is represented by the modification of the whole Raman spectrum. In Fig. 9 are compared the spectra for normal RBC obtained at 10 and 150 s exposure time, respectively. Both spectra were normalized to the highest Raman peak. As it can be seen, for long exposure a background appears and the relative bands intensities are modified. In particular, cellular photo-damage leads to spectral changing in the spin-sensitive region, where an increase of the Raman ν_{37} band is observed, indicating irreversible Hb transition to

#91619 - $15.00 USD Received 15 Jan 2008; revised 25 Feb 2008; accepted 2 Mar 2008; published 19 May 2008

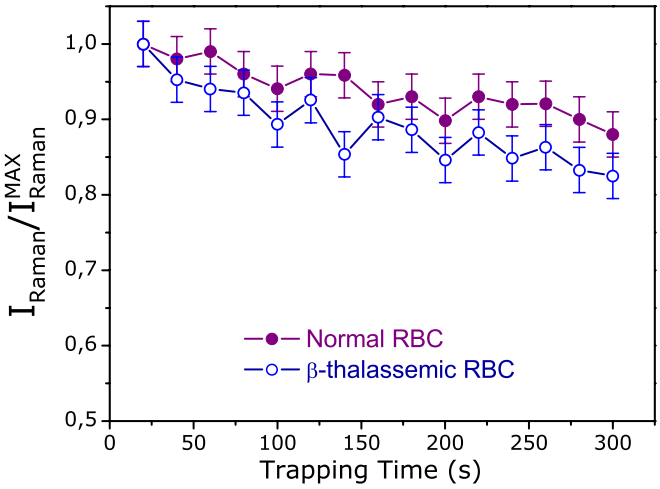

Fig. 7. Intensity of the Raman ν_{11} band, as function of the exposure-time to the trapping radiation for normal (•) and β-thalassemic (○) RBCs. The intensity values are normalized to the value at t=20 s.

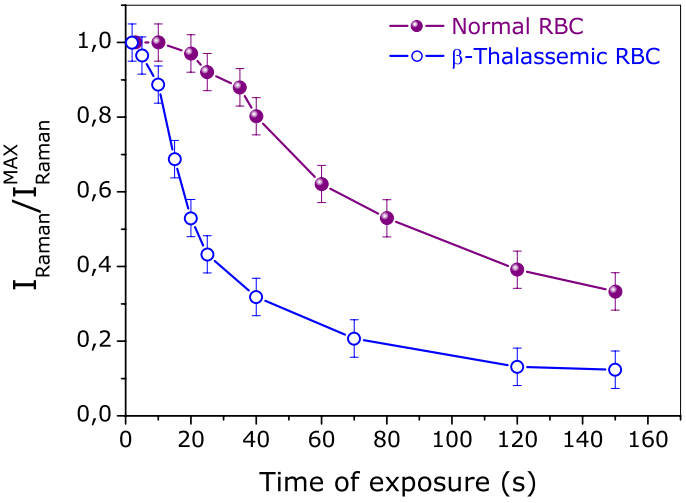

Fig. 8. Intensity of the Raman ν_{11} band, as function of the exposure-time to the Raman probe for normal (•) and β-thalassemic (○) RBCs. The intensity values are normalized to the value at t=3 s.

the met state. Similar effects have been already reported for healthy erythrocytes exposed to radiation at 514 nm and they have been attributed to protein denaturation, resulting in heme

#91619 - $15.00 USD Received 15 Jan 2008; revised 25 Feb 2008; accepted 2 Mar 2008; published 19 May 2008

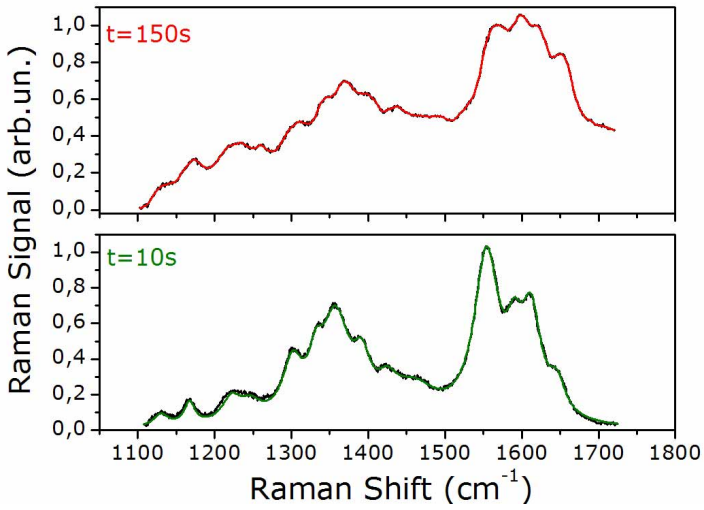

Fig. 9. The Raman spectra of a normal RBC exposed to 532 nm radiation for 10 and 150 s. Solid lines are the best fit lineshape convolutions.

aggregation within the cell [30].

3.3. Mechanical response to applied stress.

The deformation capability of RBC is mainly due to the elasticity of its membrane. This last is made of a lipidic bilayer, covering a protein network essentially composed of spectrin tetrameres linked by actin and protein 4.1 to form complex junctions. The mechanical properties of such structure has been largely investigated from both theoretical [41-43] and experimental [44-46] points of view. In the first case, the studies were devoted to develop, through computational simulations, reliable models for the architecture of the spectrin network, able to simulate the erythrocyte mechanical properties. In the second case, the investigations relied on the measurement of cellular distortion in response to an applied mechanical stress. This issue has been addressed by using many different experimental techniques, including mainly micropipette aspiration [48]. This last is based on the creation of a protrusion from the cellular membrane, which is drawn into the pipette. The relation between the protrusion extension and the pressure gives the shear elastic modulus. Recently, Hénon *et al.* [46] have measured this parameter for normal human erythrocytes by using an Optical Tweezers system: in this case, calibrated forces were applied via small silica beads bound to the RBC membrane. The necessity to use such beads arises from the need to exert known forces, in order to obtain an absolute measurement of the RBC shear modulus. Indeed, an absolute force calibration requires trapping of objects of well known shape, size, and composition. Similar measurements have been also performed by Lenormand *et al.* [45] on the free spectrin skeleton, extracted from the membrane of a RBC .

In the present work we characterize the mechanical response of t-RBCs compared to healthy ones. It is important to underline that, although thalassemic syndromes concern mainly a genetic defect in hemoglobin synthesis, precipitation of free globin chains leads to various membrane dysfunctions [49]. This is also proven by the presence of defects in morphology and shape of RBC affected by this disease.

#91619 - $15.00 USD Received 15 Jan 2008; revised 25 Feb 2008; accepted 2 Mar 2008; published 19 May 2008

Our investigation was performed by stretching single erythrocytes by using a double Optical Tweezers system. Due to the comparative character of this investigation, it was not necessary to exert the mechanical stretching by using microbeads as handles. Of course, this simplifies the measurement procedure, avoiding the difficulty to obtain RBCs with microbeads adherent to the membrane in a proper relative position [45].

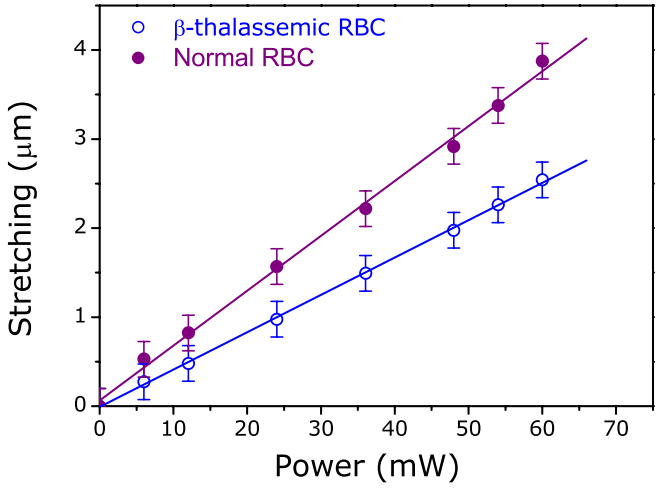

Fig. 10. Response to applied stretching for normal and abnormal RBCs.

In Fig. 10 we report the RBC elongation as function of the trapping beam power for healthy and thalassemic RBCs. Each value results from an average of 25 measurements performed on different cells. The error bars correspond to the standard deviation. The data plotted in Fig. 10 reveal a quite different mechanical response of normal cell with respect to t-RBCs. From a linear fit of the experimental data, it was possible to estimate the ratio of the shear modulus k for the two kinds of cells. This results to be: $k_n/k_\beta=0.68\pm0.05$.

If we assume $k_n=2.5\pm0.4$ pN/μm, as found by Hénon *et al.* [46], we obtain $k_\beta=3.7\pm0.9$ pN/μm. Previous measurements on β-thalassemic cells, performed with standard micropipette aspiration, brought out an elastic shear modulus in beta-thalassemia 33 % [50] higher than the normal one, against the 48% found here.

Some consideration can be done to explain this difference. First of all, as already pointed out in the ref. [46], since the two methods (double-trap and micropipette) do not operate in the same deformation regime, they are not expected to lead to the same result. Moreover, in micropipette aspiration measurements the friction force between the cellular membrane and the glass pipette wall may have a significant role in force balance.

Finally, in more than 10 % of the total measurements in β thalassemic cells, we observed an evident damage to RBCs by applying strong deformation. In such cases, the stretching caused a membrane fragmentation and a consequent cell death. In all the other cases, the vitality of normal cells was not affected, as also proved by Raman measurements performed before and after application of the mechanical stress.

#91619 - $15.00 USD Received 15 Jan 2008; revised 25 Feb 2008; accepted 2 Mar 2008; published 19 May 2008

4. Conclusions

This paper reports the characterization of heterozygous thalassemic red blood cells, at single cell level, by using a Raman Tweezers system. The study has been performed by analyzing the resonantly enhanced inelastic photons scattering from hemoglobin. Moreover, we have investigated the cellular response to mechanical stress, by using a double-trap system. Some significant difference in the functionality of these cells with respect to normal erythrocytes have been highlighted. In particular, the oxygenation capability of Hb has revealed to be reduced in β thalassemic RBCs. The two types of cells also present a different response to photo-induced oxidative stress. We have also measured the membrane shear modulus for thalassemic erythrocytes, which have revealed to be higher than 40 % with respect to healthy cells; this result indicates an even more pronounced rigidity with respect to that measured with conventional technique based on micropipette aspiration. Our results confirm medical predictions regarding thalassemia, such as the reduced oxygenation capability of t-RBCs and their higher rigidity. Moreover they provide an interesting starting point to explore the application of a Raman Tweezers system in the analysis of others blood disorders. Unlike the traditional diagnostic tools, our approach is able to provide with the same apparatus both chemical and mechanical properties, even at single RBC level. That allows to extol heterogeneity, which is instead hidden by bulk-based techniques.

It is also worth to be noted that a combined Raman Spectroscopy and double trap system opens new opportunities to study the protein rearrangement in cellular membrane under mechanical stress conditions. We think that this is a intriguing subject, which is, as far as we know, still poorly investigated [51]. At this purpose, it is useful to observe that it is possible to have at the very same time RBCs fluorescence microscopy imaging, to determine the cellular change in shape under mechanical stress application [52]. Such measurements on RBCs could provide new insight on the interaction of membrane proteins, such as spectrin and actin. Improvements in our experimental set-up are in progress to reach this goal.

Acknowledgments

The authors are grateful to Andrea Latini (Crisel Instruments, spa) for assistance with the CCD camera and to Prof. P. Russo for the critical reading of this manuscript.

#91619 - $15.00 USD Received 15 Jan 2008; revised 25 Feb 2008; accepted 2 Mar 2008; published 19 May 2008